*J Mater Sci: Mater Electron*

# Study on the strain behavior and piezoelectric properties of lead-free $Bi_{0.5}(Na_{0.8}K_{0.2})_{0.5}TiO_3$ ceramics modified with $Sn^{4+}$ ions

Nguyen Truong-Tho[1,*] and Dai Le Vuong[2]

[1] Department of Physics, College of Sciences, Hue University, Hue City, Thua Thien Hue Province, Vietnam
[2] Faculty of Natural Sciences, Thu Dau Mot University, Thu Dau Mot, Binh Duong Province, Vietnam

**Received:** 30 October 2020
**Accepted:** 16 May 2021



## ABSTRACT

The microstructure, strain behavior, and piezoelectric properties of $Bi_{0.5}(Na_{0.8}K_{0.2})_{0.5}TiO_3$ (BNKT-Sn) piezoelectric ceramics modified with $Sn^{4+}$ ions were systematically studied. The experimental results indicated that the $Sn^{4+}$ ion doping was a viable and effective method to promote the electromechanical properties and the strain behavior of the BNKT ceramics. When the Sn content was 0.02 mol, the resultant BNKT ceramics exhibited excellent electrical properties with a density of 5.92 g.cm$^{-3}$, a dielectric constant ($\varepsilon_r$) of 1235, a dielectric loss (tan$\delta$) of 0.048, the electromechanical coupling factors of 0.36 ($k_p$) and 0.39 ($k_t$), a piezoelectric coefficient ($d_{33}$) of 171 pC/N, and a mechanical quality factor ($Q_m$) of 125. Moreover, a large unipolar strain of 0.45% and a high normalized strain of 865 pm/V were achieved at 50 °C. The main achievement of this study was the large normalized strain ($d_{33}^*$) of 876 pm/V at the $SnO_2$ content of 0.04 mol.

## 1 Introduction

Lead-free piezoelectric materials with high strains exhibit an interconversion of electrical and mechanical energies that can be utilized in a wide range of applications, such as sensors, actuators, and electrical devices [1–4]. Therefore, multifarious piezoelectric ceramics, such as $K_xNa_{(1-x)}NbO_3$-based ceramics [5–8], $Bi_{0.5}(Na_{(1-x)}K_x)_{0.5}TiO_3$-based piezoelectric ceramics [1, 2, 9–11], and $(Ba_{1-x}Ca_x)(Zr_{1-y}Ti_y)O_3$-based piezoelectric ceramics [12–14] have been synthesized. Among the lead-free materials, $Bi_{0.5}(Na_{(1-x)}K_x)_{0.5}TiO_3$ (BNKT)-based ceramics are the most promising candidates for replacing the PZT-based piezoelectric ceramics due to the former's large piezoelectric coefficients, large field-induced strains, good ferroelectricity, and high Curie temperatures [15]. Furthermore, modification of the elements at A-and/or B-sites to obtain a modified BNKT solid solution is a viable approach to enhance the dielectric, ferroelectric, and piezoelectric properties or reduce the sintering temperature [16]. Zhang et al. [17] reported that the $Sn^{4+}$ cations could enter the B-sites of a perovskite structure to replace the $Ti^{4+}$ ions and

Address correspondence to E-mail: truongtho@hueuni.edu.vn

https://doi.org/10.1007/s10854-021-06215-8
Published online: 27 May 2021

enhance the energy storage density. It was also pointed out that 1% mol $SnO_2$-doped $Sr_{0.6}(Na_{0.5}Bi_{0.5})_{0.4}TiO_3$ ceramics yielded a high energy storage efficiency (η) of 80%. Recently, in our research, it was discovered that optimal Sn doping could effectively reduce the sintering temperature of the BNKT ceramics by generating a eutectic liquid phase at 170 °C [18]. Moreover, it was found that isovalent $S_n$ substitution at Ti-sites could induce a ferroelectric-to-nonpolar pseudocubic phase transition and a giant strain at the phase boundary [19, 20]. Recently, several novel BNKT-based ceramics exhibiting high strain under a low electric field have been discovered. In a research reported by Khaliq et al. [21], $Bi_{0.5}Na_{0.5}TiO_3$ seed-modified $0.96Bi_{0.5}(Na_{0.78}K_{0.22})_{0.5}TiO_3$–$0.04Bi(Mg_{0.5}Ti_{0.5})O_3$ exhibited considerably high $S_{max}/E_{max}$ values of 725 pm/V at 3 kV/mm and 560 pm/V at 2.5 kV/mm. Gupta et al. [22] recently reported that $Sr(Hf_{0.5}Zr_{0.5})O_3$-doped $Bi_{0.5}(Na_{0.8}K_{0.2})_{0.5}TiO_3$ ceramics display excellent piezoelectric properties. The ceramics with $Sr(Hf_{0.5}Zr_{0.5})O_3$ content of 2% mol showed the $S_{max}/E_{max}$ value of 663 pm/V under the field of 5 kV/mm, indicating its potential as a lead-free replacement material for actuating applications. Huo et al. [23] reported obtaining a large normalized strain of 600 pm/V in the BNKT ceramics in complex with $Cs_2Nb_4O_{11}$ tungsten bronze phase. Zhang et al. [24] also demonstrated that $(Bi_{0.5}Na_{0.5})TiO_3$-based ceramics exhibited a large strain of 0.38% ($d_{33}^* = S_{max}/E_{max}$ = 638 pm/V) under a field of 60 kV/cm. In another report by Zhang et al. [25], $d_{33}^* = S_{max}/E_{max}$ = 720 was achieved for the NKBT-0.05FN ceramic at 50 kV/cm. In the present study, Sn-modified $Bi_{0.5}(Na_{0.8}K_{0.2})_{0.5}TiO_3$ (BNKT) lead-free ceramics were synthesized using a conventional solid-state reaction method, with the main objective of improving the strain behavior and the piezoelectric properties of BNKT ceramics by adding a suitable amount of $Sn^{4+}$ ions.

## 2 Experiment

The general chemical formula of the investigated material was $Bi_{0.5}(Na_{0.8}K_{0.2})_{0.5}(Ti_{1-x}Sn_x)O_3$ (BNKTS) ($x$ = 0.0, 0.01, 0.02, 0.03, and 0.04). Reagent grade oxide powders (purity ≥ 99.5%) of $Bi_2O_3$, $TiO_2$, $Na_2CO_3$, $K_2CO_3$, and $SnO_2$ were used as starting materials. The oxide powders of $Bi_2O_3$, $TiO_2$, $Na_2CO_3$, $K_2CO_3$, and $SnO_2$ were weighed and milled for 20 h. The powders were calcined at 850 °C for 2 h, producing the BNKTS compound. The production of the BNKTS compound was confirmed through thermogravimetric analysis (TGA) and differential thermal analysis (DTA) [20]. The calcined BNKTS powder was then milled for 20 h. Next, the ground materials were pressed at 150 MPa into pellets of diameter 1.2 cm and thickness 1.5 mm by steel mold of the corresponding diameter, which was then sintered at 1100 °C for 3 h in the air at a heating/cooling rate of 5 °C/min.

The crystalline phase of the sintered ceramics was examined by X-ray diffraction (XRD, D8 Advance) under Cu-$K_\alpha$ radiation at a wavelength of 1.5405 Å, in the 2θ range of 20°–70°, and with a step size of 0.02°, at room temperature (*RT*). Scanning electron microscopy (SEM, Hitachi S_4800) was employed to examine the surface morphologies. In addition, the energy-dispersive spectrometry (EDS) of the sintered ceramic was performed. Furthermore, Rietveld refinements were performed using the FullProf software, and the grain size was determined using the mean linear intercept method. The sintered samples were coated with silver paint at 550 °C for 15 min and then polarized in silicone oil at 25–125 °C for 25 min under 3.5 kV/mm to measure their piezoelectric properties. The piezoelectric properties of the Sn-modified BNKT ceramics were determined from their resonant vibration spectra collected at room temperature using an impedance analyzer (HP 4193A and RLC Hioki 3532). The piezoelectric constant, $d_{33}$, was determined using a $d_{33}$ meter (YE2730A, Sinocera).

## 3 Results and discussion

### 3.1 The structure and microstructure characteristics

In order to clarify the morphological evolutions and the elemental distributions of the ceramic samples, the EDS spectra of the Sn-doped BNKT ceramics were obtained and are shown in Fig. 1a. It is clear from the EDS spectra that Bi, Na, K, Ti, and O elements were present in the synthesized ceramics, similar to the findings reported by Wang et al. [26]. In our recent research, the sintering temperature of the Sn-doped BNKT ceramics was determined to be 1100 °C [18]. In comparison to the green pellets

without sintering that had a diameter of 12 mm and a thickness of 1.5 mm, after sintering at 1100 °C for 3 h, the Sn-doped BNKT ceramics exhibited good shrinkage with a diameter of 10.3 mm and a thickness of 1.0 mm [inset of Fig. 1a]. Therefore, based on preliminary observation and the testing for sample homogeneity using the EDS surface method, it could be confirmed that the chemical composition of the Sn-doped BNKT ceramics was considerably good qualitatively as well as quantitatively.

Figure 1b displays the crystalline phases of the Sn-doped BNKT ceramics over a 2θ range of 20°–70°. All samples possessed a typical perovskite structure. In order to clearly illustrate the effect of $SnO_2$ on the structural properties of the BNKT ceramics, a magnified view of the peaks in the region between 46.2° and 47.1° is presented in Fig. 1c. The tetragonal phase concentration was quite low and was observed only in the ceramic samples without $Sn^{4+}$ ions or those with an extremely small concentration of $Sn^{4+}$ ions. The Lorentz curves could be used to theoretically fit the partial intensity profile of ceramics as presented in Fig. 1c. This was consistent with the report by Han et al. [27] for Sn-doped $Bi_{1/2}(Na_{0.82}K_{0.18})_{1/2}TiO_3$. Moreover, the presence of rhombohedral crystal symmetries (*R3c*) in the $Bi_{0.5}(Na_{0.8}K_{0.2})_{0.5}(Ti_{0.98}Sn_{0.02})O_3$ sample was confirmed using the Rietveld refinement technique (Fig. 1d). The fitting analysis of the peak shape, peak position, structure, and background was performed by considering the rhombohedral (*R3c*) space group symmetry. In our previous report, the coexistence of two different structural phases occurred, and hence, the morphotropic phase boundary (MPB) was confirmed at $Sn^{4+}$ ion content of 0–0.01 mol, along with the rhombohedral phase fraction (*R3c*) of greater than 60% [20]. On further refinement (the content of $Sn^{4+}$ ions was higher than 0.01 mol), the rhombohedral symmetry was observed to fit well ($M_R$ = 100%). It is well known that the $Bi_{0.5}Na_{0.5}TiO_3$ ceramic is rhombohedral, while the $Bi_{0.5}K_{0.5}TiO_3$ ceramic is tetragonal at room temperature [28]. The split $(002)_T$ and $(200)_T$ peaks indicate the ferroelectric tetragonal phase (*T*), while the single $(200)_R$ peak represents the ferroelectric rhombohedral phase (*R*). Thus, doping could increase the tetragonal or rhombohedral phases of the BNKT ceramic system. According to Pradhan et al. [29], the structure of the $Bi_{0,5}(Na_{0.8}K_{0.2})_{0,5}TiO_3$ ceramics can be described by the *P4mm* space group with the lattice parameters of $a$ = 3.893 Å and $c$ = 3.908 Å and a c/a ratio of 1.004. However, in our work, a pure $Bi_{0,5}(Na_{0.8}K_{0.2})_{0,5}TiO_3$ with both R phase (space group *R3c* ~ 60%) and T phase (space group *P4mm* ~ 40%) was observed [20]. Similar

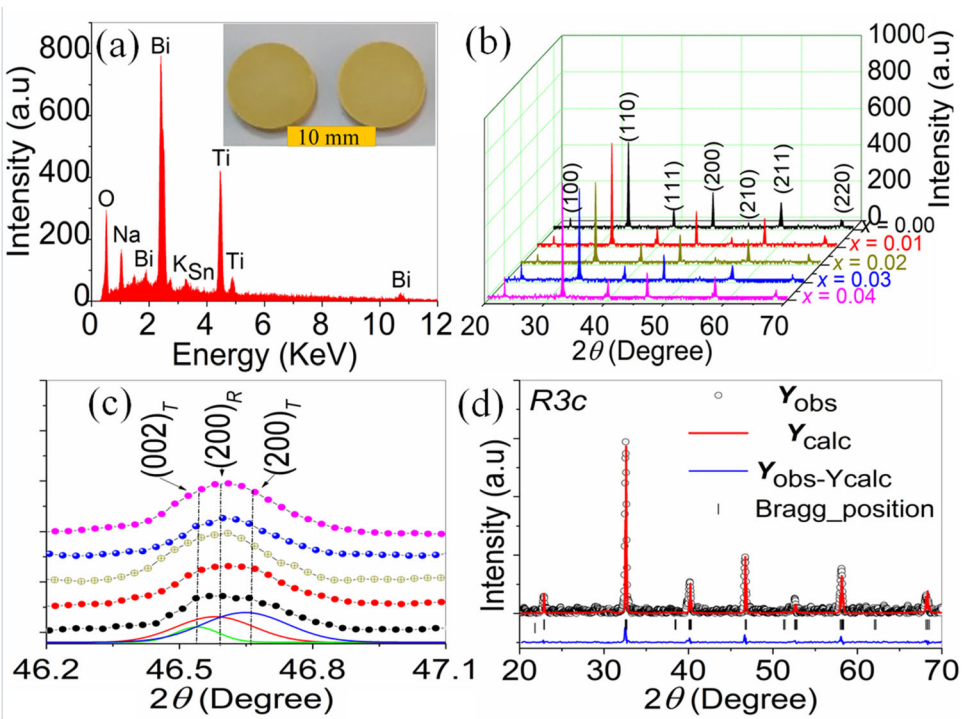


**Fig. 1** The structure of the $SnO_2$-doped BNKT ceramics

observations were reported by Ullah et al. [28], who observed that the relative amount of the tetragonal phases was 58.6% for the $Bi_{0.5}(Na_{0.78}K_{0.22})_{0.5}TiO_3$ ceramic samples sintered at 1100 °C. The overall effect of $Sn^{4+}$ ions on the XRD patterns of $Bi_{0.5}(Na_{0.8}K_{0.2})_{0.5}TiO_3$ ceramics was the slight shift in the intensity of the peaks toward lower angles and the enhancement of the rhombohedral phase (*R*) structure, as depicted in Fig. 1c. This result implies that the $Sn^{4+}$ ions (0.69 Å) replaced the similar-sized $Ti^{4+}$ ions (0.61 Å) at the B-site rather than the bigger cations at the A-site, such as $K^+$, $Na^+$, and $Bi^{3+}$ [18]. Similar results were observed by Yan et al. [30] in Sn-doped $Ba_{0.5}Sr_{0.5}TiO_3$ ceramics as well as by Zhang et al. [17] in Sn-doped $Sr_{0.6}(Na_{0.5}Bi_{0.5})_{0.4}TiO_3$ ceramics. It is evident that the Goldschmidt's tolerance factor [16], $t_{(BNKT/Sn)} \leq t_{BNKT}$ when $r_{Ti} = 0.61$ Å $< r_{Sn} = 0.69$ Å, and the corresponding atom radii are $r_{Bi^{3+}} = 1.17$ Å, $r_{Na^+} = 1.39$ Å, $r_{K^+} = 1.64$ Å, and $r_{O^{2-}} = 1.42$ Å [31, 32]. Therefore, the tolerance factor of pure BNKT was $t_{BNKT} = 0.9492$ when $t_{BNKT/Sn} \leq t_{BNKT} < 1$.

Figure 2 presents the scanning electron microscopy images of the fracture surfaces (SEM) of the Sn-doped BNKT ceramics with different Sn contents. In our previous research [18], the perovskite structure of the ceramic samples was formed in the temperature range of 745–883 °C. In order to ensure the single perovskite phase formation in high-volume samples, the calcination of the Sn-doped BNKT ceramics was carried out at 850 °C for two hours (Fig. 2a). The average grain size of the calcined BNKT compounds was about 0.33 μm (Fig. 2a). However, the mechanism underlying the effects of the preliminary calcination temperature on the microstructures of the Sn-doped BNKT samples remains unknown so far and requires further investigation. In order to better understand the influences of different Sn contents on the microstructure of the Sn-doped BNKT ceramics, the samples were sintered at 1100 °C for three hours (Fig. 2b–f). In all samples, the grains had a dense microstructure and a clear grain boundary. At low Sn doping levels ($x \leq 0.03$), the grain size increased with the increasing Sn content and reached the maximum value of 1.62 μm at the Sn content of 0.03 mol (Fig. 3e). The increase in the grain size may be due to a reaction between Bi and Sn elements, which produced some molten compounds [33, 34]. Similar behaviors of increase in the grain size and change in the morphology have also been observed in Zn-modified BNKT ceramics [35]. Muhsen et al. [36] suggested that the increase in the grain size could be related to the differences in the ionic radii of $Sn^{4+}$ and $Ti^{4+}$ at the B-sites, due to which the interdiffusion movement occurred via the grain boundary through the formation of necks between the grains, and its growth accelerated the grain growth. As the Sn content further increased, the grain size decreased (Fig. 3f). This could be because during sintering to produce the Sn-modified BNKT ceramics, a portion of $Sn^{4+}$ ions may accumulate near the grain boundaries and reduce their densification mobility. The reduction in the mobility of the grain boundary weakens the mass transport and thus inhibits the grain growth to a certain extent [37]. It is reported that a large grain size is essential to obtain ceramics with good piezoelectric properties [16, 18, 36]. $Sn^{4+}$ ions diffused into the BNKT lattice until the Sn doping content was less than 4%.

### 3.2 Influence of Sn content on the strain behavior and piezoelectric properties of BNKT ceramics

Figure 4a illustrates the dielectric constant ($\varepsilon_r$) and dielectric loss ($\tan\delta$) of the sintered ceramics with different $SnO_2$ contents at 1 kHz. With the increasing Sn content, $\varepsilon_r$ gradually increased, reached the peak value of 1235 at $x = 0.02$, and then decreased. The variation trend of $\tan\delta$ was the opposite; $\tan\delta$ decreased rapidly when the Sn content was less than 0.02 mol, reached the smallest value of 0.048 at the Sn content of 0.02 mol, and then started to increase.

These phenomena are probably related to the density and the increasing grain size. According to Muhsen et al. [36], the movement and growth of the grain boundaries through the formation of necks between the grains increase the grain size of the ceramics. The dielectric properties of the Sn-doped BNKT ceramics were improved with an increase in their density (Fig. 4b). With the increase in the Sn content from 0 to 0.04 mol, the density of the ceramics increased from 5.80 g/cm$^3$ to 5.92 g/cm$^3$, reached the maximum values of 5.92 g/cm$^3$ at $x = 0.02$ (98.6% of the theoretical density) corresponding to the highest $\varepsilon_r$ value, and then started to decrease again. This could be because the low melting point of the Bi–Sn system is beneficial for the generation of a eutectic liquid phase at 138.4 °C [33, 34], and this phase can work as a lubricant

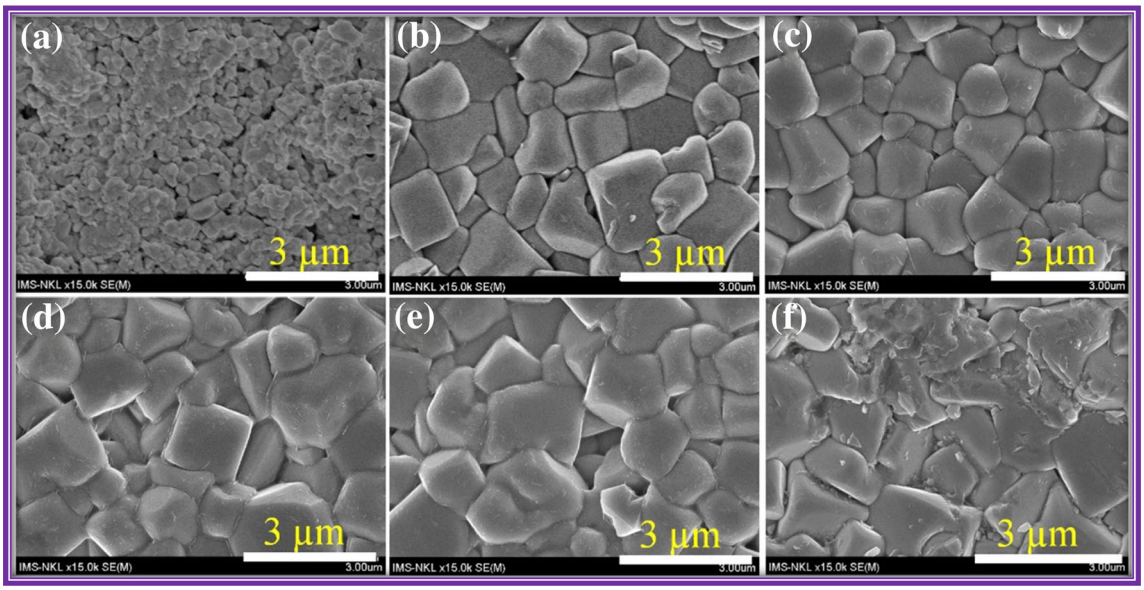


**Fig. 2** Microstructures of the Sn-doped BNKT ceramics: **a** calcined ceramic at 850 °C, **b-f** sintered ceramic at 1100 °C ( **b** $x = 0.00$, **c** $x = 0.01$, **d** $x = 0.02$, **e** $x = 0.03$, **f** $x = 0.04$)

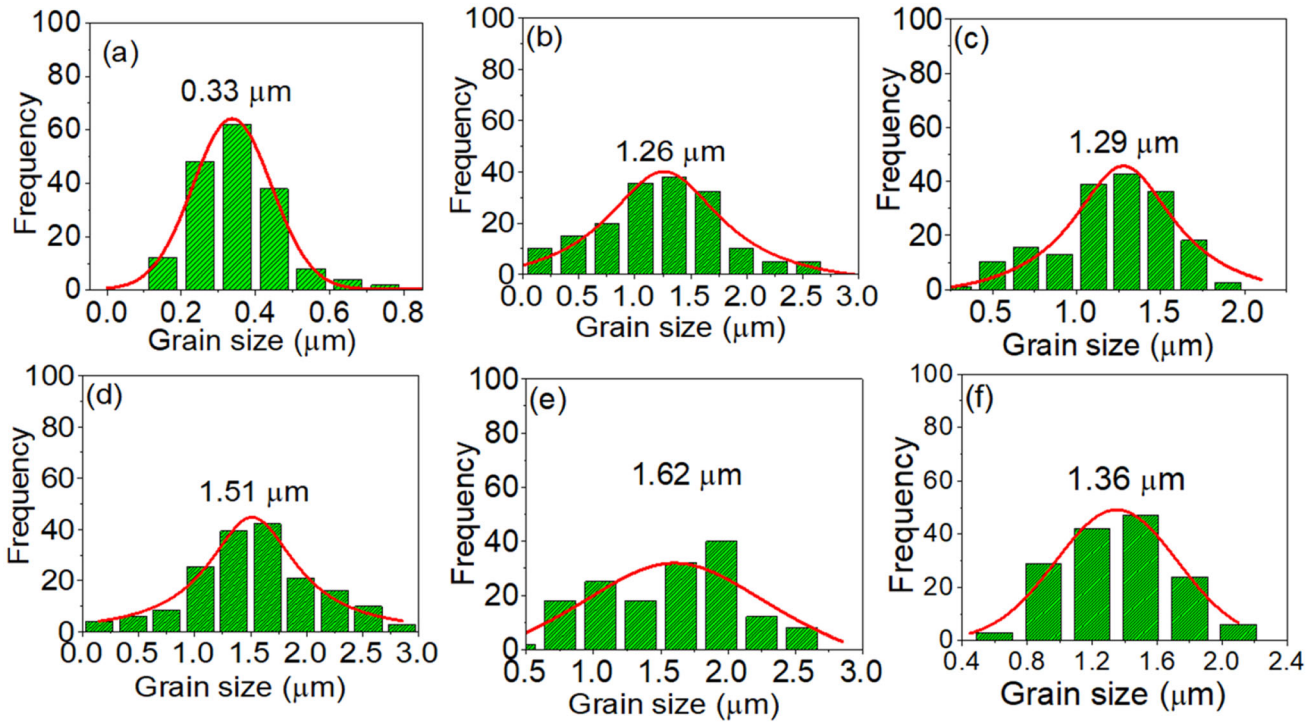


**Fig. 3** Grain size distribution for the $SnO_2$-doped BNKT ceramics: **a** calcined ceramic at 850 °C, **b–f** sintered ceramic at 1100 °C ( **b** $x = 0.00$, **c** $x = 0.01$, (d) $x = 0.02$, **e** $x = 0.03$, **f** $x = 0.04$)

during the sintering process, wetting the solid particles, and providing capillary pressure among them, thereby increasing the sintering capacity of the ceramics [3, 4, 38]. However, when the Sn content exceeded the solubility limit of the $Sn^{4+}$ ions, the segregation of some $Sn^{4+}$ ions at the grain boundaries prevented grain boundary movements during sintering and inhibited the grain growth, leading to a decrease in the grain size and a reduction in the

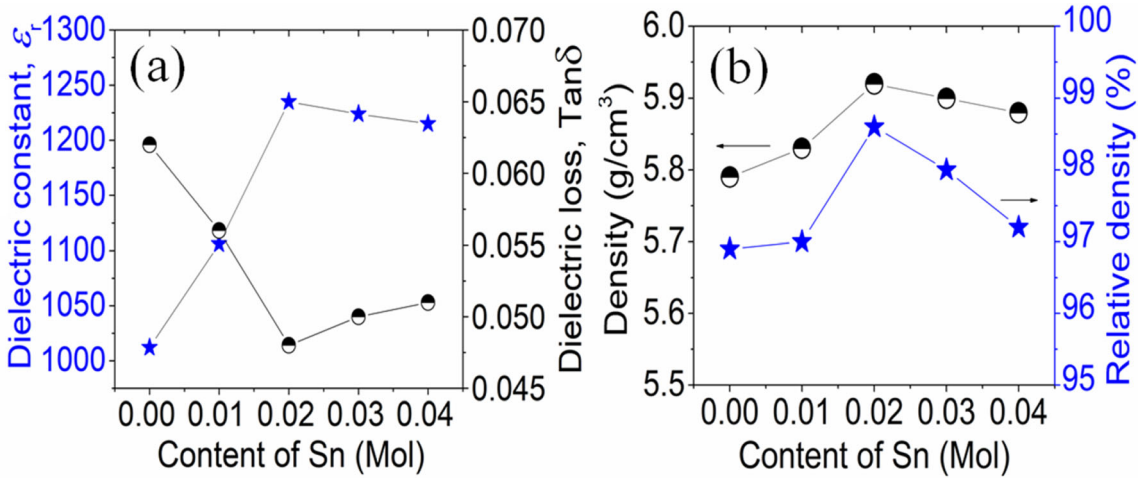


**Fig. 4** **a** The dielectric constant and dielectric loss of the Sn-doped BNKT ceramics; **b** Density of the Sn-doped BNKT ceramics

density and the dielectric properties of the ceramics [36].

The piezoelectric properties of the Sn-modified BNKT ceramics were determined from their resonant vibration spectra (Fig. 5a, b). It is clear from Fig. 5c that the electromechanical coupling factors ($k_p$, $k_t$) and the piezoelectric factor ($d_{33}$) varied as a function of the Sn content. With the increase in the Sn content, the values of $k_p$, $k_t$, and $d_{33}$ were significantly increased. At $x = 0.02$, the Sn-modified BNKT ceramics exhibited the best piezoelectric properties, with the $k_p$, $k_t$, and $d_{33}$ values of 0.36, 0.39, and 171 pC/N, respectively, and this could be attributed to the increase in the grain size. Therefore, at small Sn contents, the increase in the grain size was beneficial for the improvement of $k_p$, $k_t$, and $d_{33}$ as the increasing grain size reduced the volume fraction of the grain boundaries [36]. However, with further increase in the Sn content, the values of $k_p$, $k_t$, and $d_{33}$ decreased; this happened when the solubility limit of the $Sn^{4+}$ ions in the $Bi_{0.5}(Na_{0.8}K_{0.2})_{0.5}TiO_3$ ceramics was 0.02 mol. When the $SnO_2$ content was above 0.02 mol, excess $Sn^{2+}$ ions accumulated at the grain boundaries and abnormally influenced the piezoelectric properties. Jiang et al. [39] obtained the best piezoelectric properties with $k_p = 0.3$ in 0.2 wt% $Mn^{2+}$ doped $(Na_{0.5}K_{0.2})_{0.5}Bi_{0.5}TiO_3$. Zhang et al. [40] reported that 0.3 wt.% $Sm^{3+}$ substitution in $(Na_{0.82}K_{0.18})Bi_{0.5}TiO_3$ ceramics exhibited a high planar coupling factor ($k_p$) value of 0.22. Surprisingly, the variation in the mechanical quality factor ($Q_m$) was almost similar to that of $d_{33}$, and the optimized Sn content was 0.03 mol instead of 0.02 mol, resulting in the highest $Q_m$ value of 125 (Fig. 5b). The values of $Q_m$ increased when the Sn content increased from 98 to 125, and then decreased with a further increase in the Sn content. It is believed that mechanical loss is typically quantified in terms of the material's mechanical loss tangent (tan$\delta$) and the dielectric loss is also quantified in terms of the material's dielectric loss tangent (tan$\delta$), which occur in the material due to the inertia of the charge exchange process [41, 42], which is represented by $Q^{-1}\ m \sim \tan\delta$. Interestingly, an abrupt drop in the $Q_m$ value was observed when 0.04 mol $Sn^{4+}$ ions were doped on the B-site $Ti^{4+}$ ions. The accumulation of an excess amount of Sn ions at grain boundaries led to a reduction in the mechanical quality factor (Fig. 3f) [43]. Thus, although the average grain size of the ceramic was the largest when the Sn content reached $x = 0.03$ (1.62 μm), as depicted in Fig. 3e, the piezoelectric properties of Sn-doped BNKT ceramics reached the highest values of $k_p$, $k_t$, $d_{33}$, and $Q_m$ when $Bi_{0.5}(Na_{0.8}K_{0.2})_{0.5}TiO_3$ was doped with 2 mol.% of the Sn dopant.

Figure 6 demonstrates the bipolar strain curves of the BNKT ceramics as a function of the Sn content [44]. A slight decrease in the maximum strain ($S_{max}$) occurred initially at $x = 0.01$; then, the $S_{max}$ value increased with a further increase in the Sn content (Fig. 7a). The value of $S_{neg}$ increased with the increasing Sn content and reached the maximum value of 0.16% at $x = 0.02$. Negative strains in ferroelectric materials manifest as the switching back point of domain reorientation under cyclic fields; hence, the highest values of $k_p$ and $d_{33}$ were obtained

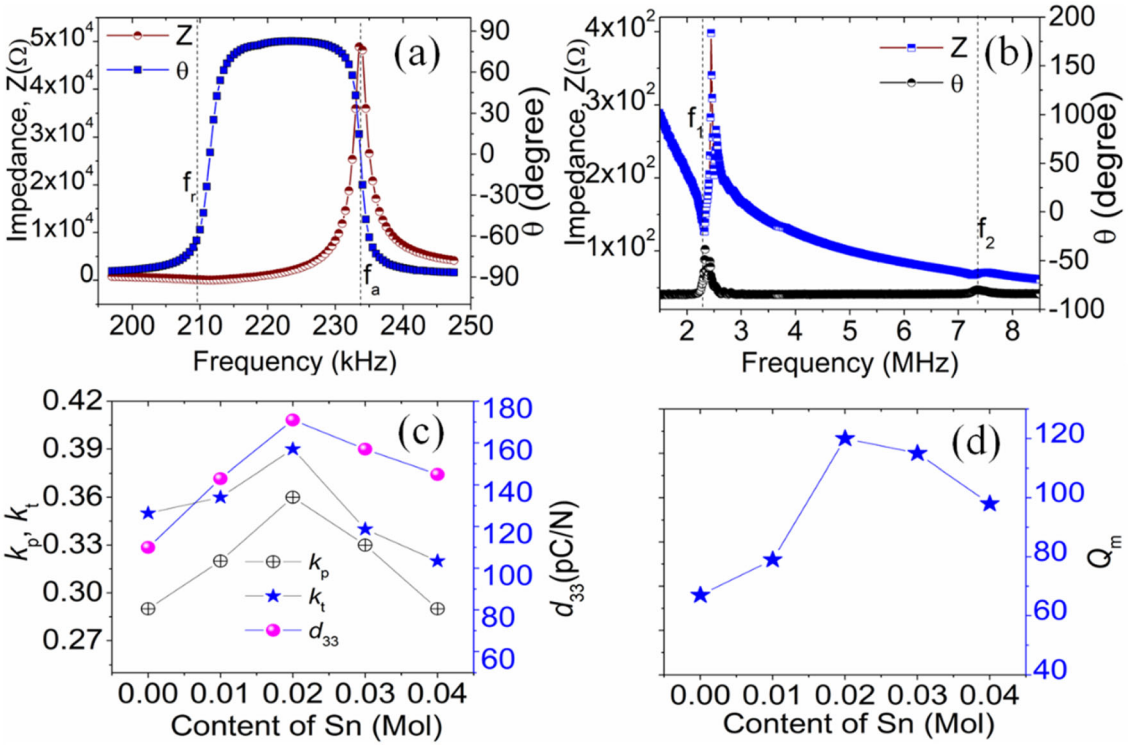


**Fig. 5** **a** Radial and **b** Thickness resonant spectra of $Bi_{0.5}(Na_{0.8}K_{0.2})_{0.5}(Ti_{0.98}Sn_{0.02})O_3$ ceramics; **c** The values $k_p$, $k_t$, and $d_{33}$; **d** The values of $Q_m$ as a function of Sn doping

at $x = 0.02$. However, with further increase in the Sn content, the $S_{neg}$ value decreased and tended to zero because the relaxor of the Sn-doped BNKT ceramics was enhanced [44]. The normalized strains ($d_{33}$*) of the sintered ceramics were calculated (Fig. 7a) and compared with those of the other BNKT-based piezoceramics (Fig. 7b). It is evident from Fig. 7a that the normalized strain reached the maximum value of 876 pm/V at $x = 0.04$ and then decreased. Therefore, the variation of the normalized strain with the Sn content was almost similar to that of $S_{max}$, and the optimized Sn content of 0.04 mol led to the largest $d_{33}$* value of 876 pm/V (Fig. 7a). Among all the BNKT-based ceramics reported to date, the BNKT-0.04Sn ceramic has the largest $d_{33}$* value of 876 pm/V (Fig. 7b) [45–50].

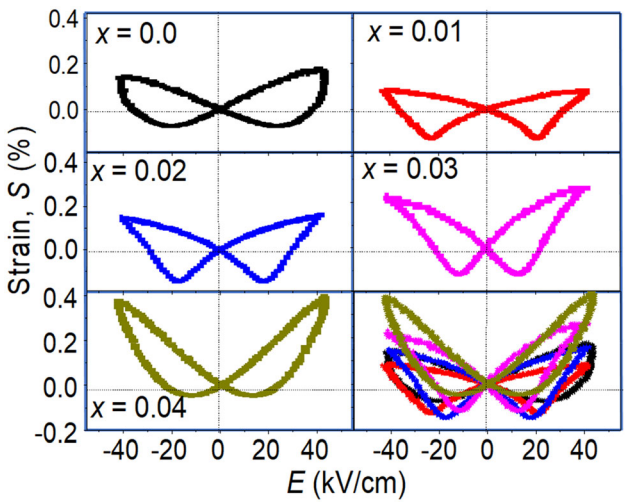


**Fig. 6** The bipolar $S - E$ loop of BNKT ceramics as a function of Sn doping

### 3.3 Influence of temperature on the strain behavior and piezoelectric properties of BNKT ceramics

For practical applications of piezoelectric materials, the temperature stability of their electromechanical properties (poling temperature and operating temperature) is crucial. In order to determine the optimum poling temperature for the Sn-doped BNKT ceramics to enhance their piezoelectric responses, their poling temperatures were measured in silicone oil under 3.5 kV/mm for 25 min (Fig. 8). At the poling temperature of 75 °C, BNKT-0.02Sn exhibited the best piezoelectric properties with $d_{33} = 171$ pC/N and $k_p = 0.36$. The effect of temperature allowed the

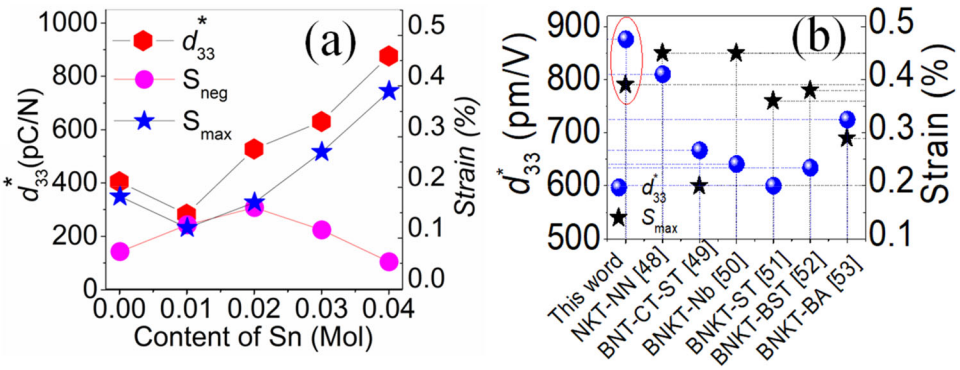


**Fig. 7** **a** Maximum strain ($S_{max}$), negative strain ($S_{neg}$), normalized strain ($d_{33}$*) versus Sn content; **b** Comparison of $S_{max}$ and $d_{33}$* values among the reported BNKT-based bulk ceramics

flexible domains to easily move in the field direction and resulted in improved piezoelectric properties. The suitable polarization of the Sn-doped BNKT ceramics was noticed in the temperature range of 50–100 °C, which then decreased quickly upon further increasing the temperature [51–53]. With a further increase in the temperature, the rise of the leakage current caused a reduction in $d_{33}$ and $k_p$ [12], which proves that the piezoelectric responses of the ceramics were dependent on the poling temperature.

Figure 9 displays the temperature-dependent strain hysteresis loops of the $Bi_{0.5}(Na_{0.8}K_{0.2})_{0.5}(Ti_{0.98}Sn_{0.02})O_3$ ceramics ($x$ = 0.02). A typical ferroelectric behavior was noticed until 100 °C. However, when the temperature exceeded $T_{F\text{-}R}$ (Fig. 10) and reached 125 °C, a little negative strain was observed [48]. Several researchers have suggested that the shift of $T_{F\text{-}R}$ in various lead-free BNKT ceramics could be related to the loss of Bi, K, and/or Na during the processing [20]. It is believed that the origin of the large strain in Bi-based ceramics is associated with the reversible electric field-induced phase transition from a nonpolar ergodic relaxor to the polar ferroelectric state [22]. Therefore, the temperature dependence of the polarization and the strain hysteresis are the maximum at the boundary where the ferroelectric state transforms into the relaxor state.

In order to elucidate the variation trend of temperature-dependent strains, strain values were plotted against temperatures ranging from 25 °C to 125 °C (Fig. 11). The temperature-induced phase transition of the ceramics was verified by the strain–electric field (S–E) hysteresis measurements. The positive maximum strain ($S_{max}$) gradually increased with temperature, reached the highest value of 0.45% at 50 °C, and then gradually decreased (Fig. 11). With further increase in temperature, lattice softening occurred when the temperature approached the phase transition temperature; hence, the $S_{max}$ value decreased [54]. When the sintering temperature was higher than $T_{F\text{-}R}$, a notable increase in the usable strain occurred due to the reduction in the remanent strain (Fig. 9). According to Yin et al. [55], $S_{max}$ reached the maximum value and $S_{neg}$ dropped to almost zero at around $T_{F\text{-}R}$, indicating that the field-induced long-range ferroelectric order disappeared around this temperature.

It is evident from Fig. 11b that $Bi_{0.5}(Na_{0.8}K_{0.2})_{0.5}(Ti_{0.98}Sn_{0.02})O_3$ ceramic presented the highest $d_{33}$* value of 865 pm/V at 50 °C. The positive maximum strain ($S_{max}$) gradually increased with increasing temperature and promoted the increase in $d_{33}$* according to the following formula: $d_{33}^* = S_{max}/E_{max}$ [45, 51]. The obtained $d_{33}$* and $S_{max}$ values in this research are higher than those reported previously for lead-free ceramics [19]. The large $S_{max}$ value can be attributed to the reversible electric field-induced transition between the ergodic relaxor and the ferroelectric status around the $T_{F\text{-}R}$ temperature [48].

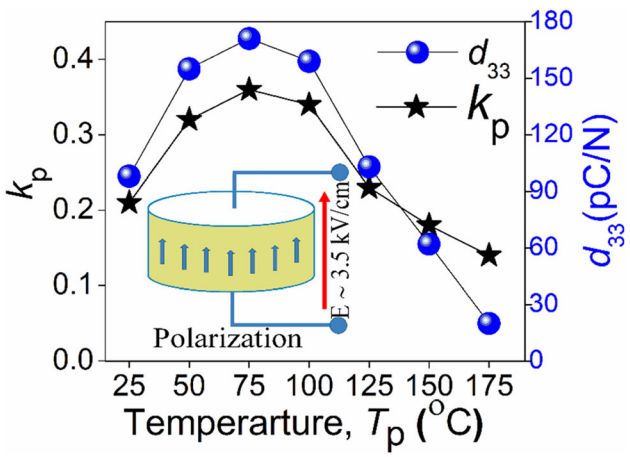


**Fig. 8** Poling temperature dependence of BNKT-0.02Sn ceramics

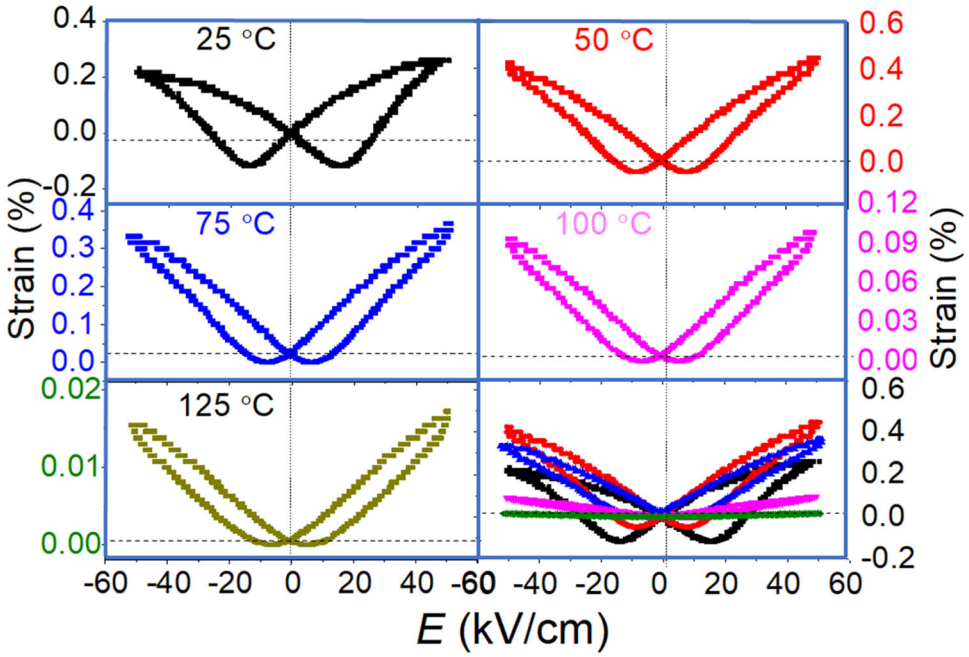


**Fig. 9** Plots of strain vs. electric field for $Bi_{0.5}(Na_{0.8}K_{0.2})_{0.5}(Ti_{0.98}Sn_{0.02})O_3$ ceramics at various temperatures

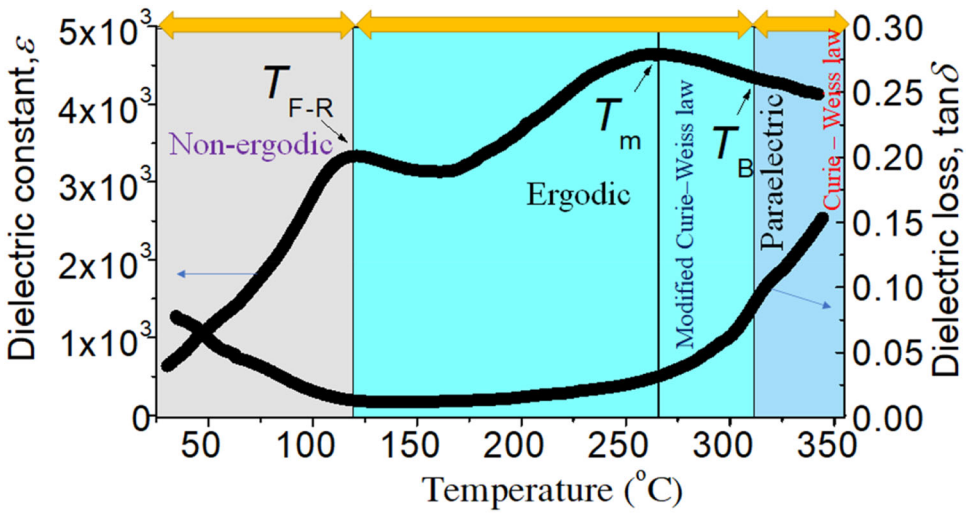


**Fig. 10** Temperature dependence of the dielectric constant and the loss of $Bi_{0.5}(Na_{0.8}K_{0.2})_{0.5}(Ti_{0.98}Sn_{0.02})O_3$ ceramics as the functions of temperature, measured at 1 kHz

Due to the shift of $T_{F\text{-}R}$ below the room temperature (*RT*), a large $d_{33}$* was obtained at *RT*.

## 4 Conclusions

In this work, $Bi_{0,5}(Na_{0.8}K_{0.2})_{0,5}(Ti_{1-x})Sn_x)O_3$ lead-free ceramics were synthesized using a conventional mixed-oxide approach. The experimental results revealed that the doping of $Sn^{4+}$ ions into the BNKT ceramics significantly improved their dielectric and piezoelectric properties as well as their strain behavior. The resultant ceramics exhibited excellent dielectric properties with a density of 5.92 $g.cm^{-3}$, a dielectric constant ($\varepsilon_r$) of 1235, and a dielectric loss (tan$\delta$) of 0.048. Under the optimized poling temperature, the sintered ceramics had the best piezoelectric constant ($d_{33}$) of 171 pC/N, while the electromechanical coupling factors were 36% ($k_p$) and 39% ($k_t$) at 75 °C. In particular, the electric field-induced

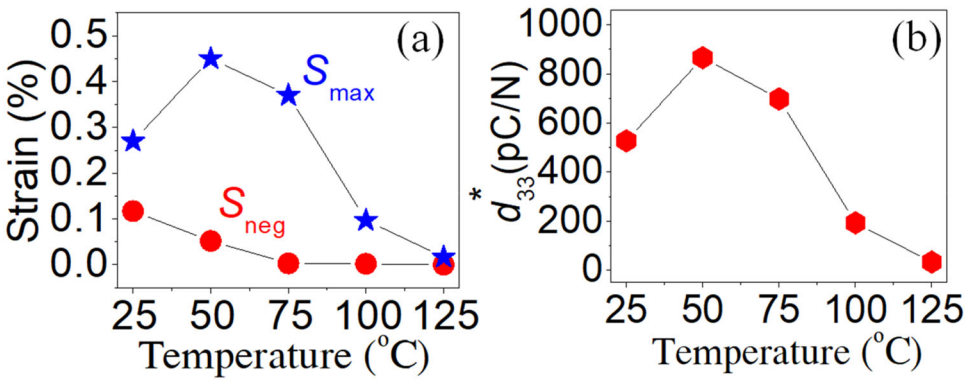


**Fig. 11** **a** $S_{max}$ and $S_{neg}$ and **b** $d_{33}$* as a function of temperature

unipolar strain was increased from 0.17% for the pure BNKT ($x$ = 0.00) to 0.45% ($x$ = 0.02) at an electric field of 50 kV/cm, with a corresponding increase in the large normalized strain ($d_{33}^*$) from 400 to 876 pm/V for 4 mol. % Sn-modified BNKT ceramic, which is relevant for the actuator applications of this material.

## Acknowledgements

This research was funded by Ministry of Education and Training under grant number B2019-DHH-13

## Author contributions

All persons who meet authorship criteria are listed as authors, and all the authors certify that they have participated sufficiently in the work to take public responsibility for the content, including participation in the concept, design, analysis, writing, or revision of the manuscript.

## References

1. L.D. Vuong, D.A. Quang, P. Van Quan, N. Truong-Tho, J. Electron. Mater. **49**(11), 6465–6473 (2020)
2. L.D. Vuong, D.A. Quang, V.T. Tung, N.H. Chuc, N.N. Trac, J. Mater. Sci.: Mater. Electron. **31**(20), 18056–18069 (2020)
3. L.D. Vuong, P.D. Gio, N.D.V. Quang, T.D. Hieu, T.P. Nam, J. Electron. Mater. **47**(10), 5944–5951 (2018)
4. L.D. Vuong, V.T. Tung, P.D. Gio, The Investigation on the Fabrication and Characterization of the Multicomponent Ceramics Based on PZT and the Relaxor PZN-PMnN Ferroelectric Materials, Ceramic Materials, IntechOpen2020
5. X. Lv, J. Wu, X.-X. Zhang, Chem. Eng. J. **402**, 126215 (2020)
6. W. Wu, J. Ma, B. Wu, Q. Gou, M. Chen, J. Alloys Compds. **822**, 153585 (2020)
7. Y. Pan, X. Dai, J. Li, Y. Yi, Y. Yu, C. He, Y. Liu, Y. Xiang, Y. Chen, Phys. Scr. **95**(6), 065802 (2020)
8. P.D. Gio, H.Q. Viet, L.D. Vuong, Int. J. Mater. Res. **109**(11), 1071–1076 (2018)
9. D.V. Le, A.Q. Dao, J. Electroceram. **44**(1), 68–77 (2020)
10. X. Zhao, W. Bai, Y. Ding, L. Wang, S. Wu, P. Zheng, P. Li, J. Zhai, J. Eur. Ceram. Soc. **40**(13), 4475–4486 (2020)
11. W. Kang, Y. Li, Z. Zheng, R. Zhao, Ceram. Int. **46**(11 Part A), 18089–18095 (2020)
12. D.A. Tuan, V.T. Tung, L.D. Vuong, N.H. Yen, L.T.U. Tu, Journal of Elec Materi **47**(10), 6297–6301 (2018)
13. D.A. Tuan, L.D. Vuong, V.T. Tung, N.N. Tuan, N.T. Duong, J. Ceram. Process. Res. **19**(1), 32–36 (2018)
14. S. Shi, H. Hashimoto, T. Sekino, Ceram. Int. **47**(3), 3272–3278 (2020)
15. J. Rödel, W. Jo, K.T.P. Seifert, E.M. Anton, T. Granzow, D. Damjanovic, J. Am. Ceram. Soc. **92**(6), 1153–1177 (2009)
16. L.D. Vuong, P.D. Gio, J. Alloys Compds. **817**, 152790 (2020)
17. L. Zhang, Z. Wang, Y. Li, P. Chen, J. Cai, Y. Yan, Y. Zhou, D. Wang, G. Liu, J. Eur. Ceram. Soc. **39**(10), 3057–3063 (2019)
18. N. Truong-Tho, L.D. Vuong, J. Adv. Dielectr. **10**(04), 2050011 (2020)
19. J.-S. Lee, K.-N. Pham, H.-S. Han, H.-B. Lee, V.D.N. Tran, J. Korean Phys. Soc. **60**(2), 212–215 (2012)
20. N. Truong-Tho, J. Electroceram. (2020). https://doi.org/10.1007/s10832-020-00224-5
21. A. Khaliq, M. Sheeraz, A. Ullah, J.S. Lee, C.W. Ahn, I.W. Kim, Sens. Actuators A **258**, 174–181 (2017)
22. S.K. Gupta, R. McQuade, B. Gibbons, P. Mardilovich, D.P. Cann, J. Appl. Phys. **127**(7), 074104 (2020)
23. Z. Huo, H. Wang, J. Xu, G. Rao, J. Wang, C. Zhou, C. Yuan, Ceram. Int. **46**(8), 10067–10074 (2020)
24. H. Zhang, P. Xu, E. Patterson, J. Zang, S. Jiang, J. Rödel, J. Eur. Ceram. Soc. **35**(9), 2501–2512 (2015)
25. Y. Zhang, P. Fan, H. Fan, B. Ye, G. Zhang, S. Jiang, H. Zhang, J. Electroceram. **44**(1), 32–40 (2020)

26. T. Wang, X.-M. Chen, Y.-Z. Qiu, Ferroelectrics **510**(1), 161–169 (2017)
27. H.-S. Han, W. Jo, J.-K. Kang, C.-W. Ahn, I. Won Kim, K.-K. Ahn, J.-S. Lee, J. Appl. Phys. **113**(15), 154102 (2013)
28. A. Ullah, C.W. Ahn, A. Hussain, I.W. Kim, Curr. Appl. Phys. **10**(6), 1367–1371 (2010)
29. L.K. Pradhan, R. Pandey, S. Kumar, S. Kumari, M. Kar, J. Mater. Sci.: Mater. Electron. **30**(10), 9547–9557 (2019)
30. Y. Yan, Q. Wu, Y. Yang, L. Zhang, H. Lin, G. Xue, X. Liu, Y. Chen, J. Yang, G. Liu, Ferroelectrics **520**(1), 171–176 (2017)
31. Y. Tsur, T.D. Dunbar, C.A. Randall, J. Electroceram. **7**(1), 25–34 (2001)
32. S.K. Ghosh, V. Chauhan, A. Hussain, S.K. Rout, Ferroelectrics **517**(1), 97–103 (2017)
33. I. Manasijević, L. Balanović, T.H. Grgurić, D. Minić, M. Gorgievski, Mater. Res. (2018). https://doi.org/10.1590/1980-5373-mr-2018-0501
34. J. Vizdal, M.H. Braga, A. Kroupa, K.W. Richter, D. Soares, L.F. Malheiros, J. Ferreira, Calphad **31**(4), 438–448 (2007)
35. L.D. Vuong, N. Truong-Tho, J. Electron. Mater. **46**(11), 6395–6402 (2017)
36. K.N.D.K. Muhsen, R.A.M. Osman, M.S. Idris, M.H.H. Jumali, N.H.B. Jamil, J. Mater. Sci.: Mater. Electron. **30**(23), 20654–20664 (2019)
37. W. Li, J. Hao, J. Du, P. Fu, W. Sun, C. Chen, Z. Xu, R. Chu, J. Adv. Ceram. **9**(1), 72–82 (2020)
38. P.D. Gio, H.T.T. Hoa, J. Mater. Sci. Chem. Eng. **2**(11), 20 (2014)
39. X.P. Jiang, L.Z. Li, F.L. Jiang, Y.Y. Zheng, L.H. Liu, Effects of Mn-doping on the piezoelectric and ferroelectric properties of (Na0. 8K0. 2) 0.5 Bi0. 5TiO3 ceramics, Trans Tech Publ, pp. 69–71.
40. Y. Zhang, R. Chu, Z. Xu, J. Hao, Q. Chen, F. Peng, W. Li, G. Li, Q. Yin, J. Alloy. Compd. **502**(2), 341–345 (2010)
41. M.G.S. Ali, N.Z. Elsyed, A.M. Abdel Fattah, G.A. Ali, *Journal of Computational Electronics* **11**(2), 196–202 (2012).
42. H. Chen, B. Tang, C. Zhong, Y. Yuan, Y. Tan, S. Zhang, Ceram. Int. **43**(10), 7383–7386 (2017)
43. L.D. Vuong, P.D. Gio, J. Mod. Phys. **5**(14), 1258–1263 (2014)
44. Z. Huo, H. Xie, J. Xu, L. Yang, W. Qiu, X. Zhang, C. Zhou, H. Wang, Front. Mater. **7**, 8 (2020)
45. G. Dong, H. Fan, J. Shi, M. Li, J. Am. Ceram. Soc. **98**(4), 1150–1155 (2015)
46. H.T.K. Nguyen, T.A. Duong, F. Erkinov, H. Kang, B.W. Kim, C.W. Ahn, H.-S. Han, J.-S. Lee, J. Korean Ceram. Soc. **57**(5), 570–577 (2020)
47. K.-N. Pham, A. Hussain, C.W. Ahn, W.K. Ill, S.J. Jeong, J.-S. Lee, Mater. Lett. **64**(20), 2219–2222 (2010)
48. K. Wang, A. Hussain, W. Jo, J. Rödel, J. Am. Ceram. Soc. **95**(7), 2241–2247 (2012)
49. A. Ullah, R.A. Malik, A. Ullah, D.S. Lee, S.J. Jeong, J.S. Lee, I.W. Kim, C.W. Ahn, J. Eur. Ceram. Soc. **34**(1), 29–35 (2014)
50. D.S. Lee, D.H. Lim, M.S. Kim, K.H. Kim, S.J. Jeong, Appl. Phys. Lett. **99**(6), 062906 (2011)
51. S.-J. Jeong, D.-S. Lee, M.-S. Kim, S.-M. Jang, I.-S. Kim, S. Mohsin, J.-S. Song, J. Electroceram. **33**(3–4), 230–238 (2014)
52. K. Kumar, B.K. Singh, M.K. Gupta, N. Sinha, B. Kumar, Ceram. Int. **37**(8), 2997–3004 (2011)
53. H. He, W. Lu, J.A.S. Oh, Z. Li, X. Lu, K. Zeng, L. Lu, ACS Appl. Mater. Interfaces **12**(27), 30548–30556 (2020)
54. P. Li, Y. Huan, W. Yang, F. Zhu, X. Li, X. Zhang, B. Shen, J. Zhai, Acta Mater. **165**, 486–495 (2019)
55. J. Yin, Y. Wang, Y. Zhang, B. Wu, J. Wu, Acta Mater. **158**, 269–277 (2018)

# Terms and Conditions

Springer Nature journal content, brought to you courtesy of Springer Nature Customer Service Center GmbH (“Springer Nature”).
Springer Nature supports a reasonable amount of sharing of research papers by authors, subscribers and authorised users (“Users”), for small-scale personal, non-commercial use provided that all copyright, trade and service marks and other proprietary notices are maintained. By accessing, sharing, receiving or otherwise using the Springer Nature journal content you agree to these terms of use (“Terms”). For these purposes, Springer Nature considers academic use (by researchers and students) to be non-commercial.
These Terms are supplementary and will apply in addition to any applicable website terms and conditions, a relevant site licence or a personal subscription. These Terms will prevail over any conflict or ambiguity with regards to the relevant terms, a site licence or a personal subscription (to the extent of the conflict or ambiguity only). For Creative Commons-licensed articles, the terms of the Creative Commons license used will apply.
We collect and use personal data to provide access to the Springer Nature journal content. We may also use these personal data internally within ResearchGate and Springer Nature and as agreed share it, in an anonymised way, for purposes of tracking, analysis and reporting. We will not otherwise disclose your personal data outside the ResearchGate or the Springer Nature group of companies unless we have your permission as detailed in the Privacy Policy.
While Users may use the Springer Nature journal content for small scale, personal non-commercial use, it is important to note that Users may not:

1. use such content for the purpose of providing other users with access on a regular or large scale basis or as a means to circumvent access control;
2. use such content where to do so would be considered a criminal or statutory offence in any jurisdiction, or gives rise to civil liability, or is otherwise unlawful;
3. falsely or misleadingly imply or suggest endorsement, approval , sponsorship, or association unless explicitly agreed to by Springer Nature in writing;
4. use bots or other automated methods to access the content or redirect messages
5. override any security feature or exclusionary protocol; or
6. share the content in order to create substitute for Springer Nature products or services or a systematic database of Springer Nature journal content.

In line with the restriction against commercial use, Springer Nature does not permit the creation of a product or service that creates revenue, royalties, rent or income from our content or its inclusion as part of a paid for service or for other commercial gain. Springer Nature journal content cannot be used for inter-library loans and librarians may not upload Springer Nature journal content on a large scale into their, or any other, institutional repository.
These terms of use are reviewed regularly and may be amended at any time. Springer Nature is not obligated to publish any information or content on this website and may remove it or features or functionality at our sole discretion, at any time with or without notice. Springer Nature may revoke this licence to you at any time and remove access to any copies of the Springer Nature journal content which have been saved.
To the fullest extent permitted by law, Springer Nature makes no warranties, representations or guarantees to Users, either express or implied with respect to the Springer nature journal content and all parties disclaim and waive any implied warranties or warranties imposed by law, including merchantability or fitness for any particular purpose.
Please note that these rights do not automatically extend to content, data or other material published by Springer Nature that may be licensed from third parties.
If you would like to use or distribute our Springer Nature journal content to a wider audience or on a regular basis or in any other manner not expressly permitted by these Terms, please contact Springer Nature at

onlineservice@springernature.com